

The landscape of tumors-infiltrate immune cells in papillary thyroid carcinoma and its prognostic value

Yanyi Huang^{1,2,*}, Tao Yi^{3,*}, Yushu Liu^{1,2}, Mengyun Yan^{1,4}, Xinli Peng⁵ and Yunxia Lv¹

¹ Department of Thyroid Surgery, Second Affiliated Hospital of Nanchang University, Nanchang, Jiangxi, China

² Nanchang University, The Second Clinical Medicine College, Nanchang, Jiangxi, China

³ Department of Otolaryngology, People's Hospital of Yichun, Yichun, Jiangxi, China

⁴ Nanchang University, The First Clinical Medicine College, Nanchang, Jiangxi, China

⁵ Department of Otolaryngology, First Affiliated Hospital of Nanchang University, Nanchang, Jiangxi, China

* These authors contributed equally to this work.

ABSTRACT

Introduction: Thyroid cancer is a very common malignant tumor in the endocrine system, while the incidence of papillary thyroid carcinoma (PTC) throughout the world also shows a trend of increase year by year. In this study, we constructed two models: ICIScore and Riskscore. Combined with these two models, we can make more accurate and reasonable inferences about the prognosis of PTC patients.

Methods: We selected 481 PTC samples from TCGA and 147 PTC samples from GEO (49 samples in [GSE33630](#), 65 samples in [GSE35570](#) and 33 samples in [GSE60542](#)). We performed consistent clustering for them and divided them into three subgroups and screened differentially expressed genes from these three subgroups. Then we divided the differential genes into three subtypes. We also distinguished the up-regulated and down-regulated genes and calculated ICIScore for each PTC sample. ICIScore consists of two parts: (1) the PCAu was calculated from up-regulated genes. (2) the PCAd was calculated from down-regulated genes. The PCAu and PCAd of each sample were the first principal component of the relevant gene. What's more, we divided the patients into two groups and constructed mRNA prognostic signatures. Additionally we also verified the independent prognostic value of the signature.

Results: Though ICIScore, we were able to observe the relationship between immune infiltration and prognosis. The result suggests that the activation of the immune system may have both positive and negative consequences. Though Riskscore, we could make more accurate predictions about the prognosis of patients with PTC. Meanwhile, we also generated and validated the ICIScore group and Riskscore group respectively.

Conclusion: All the research results show that by combining the two models constructed, ICIScore and Riskscore, we can make a more accurate and reasonable inference about the prognosis of patients with clinical PTC patients. This suggests that we can provide more effective and reasonable treatment plan for clinical PTC patients.

Submitted 15 December 2020

Accepted 29 April 2021

Published 21 May 2021

Corresponding author

Yunxia Lv, 83394045@qq.com

Academic editor

Kenta Nakai

Additional Information and
Declarations can be found on
page 20

DOI [10.7717/peerj.11494](#)

© Copyright

2021 Huang et al.

Distributed under

Creative Commons CC-BY 4.0

OPEN ACCESS

Subjects Bioinformatics, Computational Biology, Immunology, Oncology

Keywords Papillary thyroid carcinoma, Tumors-infiltrate immune cells, Prognostic model

INTRODUCTION

Thyroid cancer is the most common malignancy of the endocrine system (*Cabanillas, McFadden & Durante, 2016*), and the global incidence of papillary thyroid carcinoma (PTC) has continued to increase annually, making it a hotspot for research on tumors of the endocrine system. PTC accounts for more than 70% of thyroid malignancies (*Lloyd, Buehler & Khanafshar, 2011*). Generally, PTC patients have a good survival prognosis, with less than a 2% mortality rate after 5 years (*Abdullah et al., 2019*). Therefore, more detailed classifications of PTC patients and targeted treatment can improve the quality of life for these patients.

The immune system plays an important role in the occurrence and development of tumors (*Scouten & Francis, 2006*). On one hand, the immune system prevents the occurrence and development of tumors by monitoring and removing tumor cells. On the other hand, the immune system's ability to clear tumor cells decreases due to various factors and as a tumor develops. Therefore, tumor-infiltrating immune cells are closely associated with tumor development. In particular, the interaction between immune cells and cancer cells contributes to the occurrence and development of cancer (*Crespo et al., 2013*). The immune system also plays a significant role in potentially screening, controlling, and treating tumors. Additionally, immunotherapy that targets CTLA-4 and PD-L1 checkpoint blocking antibodies (*Varricchi et al., 2019*) can improve the prognoses of patients with multiple malignancies. Therefore, immunotherapy is considered an effective tumor treatment method with good synergistic survival benefits across a variety of cancers (*Antonelli, Ferrari & Fallahi, 2018*). However, due to the limitations of this treatment, it is necessary to investigate novel therapeutic markers that could determine PTC subgroups for immunotherapy treatment.

Previous studies have classified the immune subtypes of thyroid cancer (*Xie et al., 2020; Zhi et al., 2020*) and grouped risk scores (*Zhuang et al., 2020*), but no comprehensive analysis or comparison of the two approaches have been conducted. This study is the first to focus on these approaches and use them to construct two signatures: ICIScore and Riskscore. ICIScore is the immune signature with lymphocyte infiltration estimation ability while Riskscore is the prognosis signature with disease-free survival (DFS) prediction. Using these two models, we can make more accurate and reasonable inferences about the prognoses of PTC patients. In this study, we also explored the correlation between tumor immune cell infiltration and DFS in tumor patients. Immune systems can show favorable or adverse outcomes, which are exhibited in the form of pro-tumor or anti-tumor activity (*Chen et al., 2019; Chen & Mellman, 2017*). The results of this study provide a new way to analyze the DFS of tumor patients.

MATERIALS AND METHODS

Data sources and processing

We downloaded clinical and RNA sequencing (RNA-seq) data (Fragments Per Kilobase Million (FPKM) values) about PTC from the Cancer Genome Atlas (TCGA) database

(<https://portal.gdc.cancer.gov/>). From these data, we selected 481 patients with an effective DFS (*Kanazawa & Kammori, 2019*) for our study. DFS refers to the time from randomization when the disease recurred or when the patient died as a result of disease progression. The microarray datasets (*GSE35570*, *GSE33630*, and *GSE60542*) were downloaded from the Gene Expression Omnibus (GEO) database (<https://www.ncbi.nlm.nih.gov/geo/>). We used the “ComBat” algorithm (*Mansbach et al., 2020*) to reduce the batch effects from non-biological technical biases between *GSE35570*, *GSE33630*, and *GSE60542*. We combined these three datasets and referred to them as the GEO combined sets.

Consistent clustering of tumor-infiltrating immune cells

Using previous pan-cancer analyses (*Charoentong et al., 2017*), we obtained a gene set of 28 tumor-infiltrating immune cells. We used a Single Sample Gene Set Enrichment Analysis (ssGSEA) algorithm (*Yi et al., 2020*) and the ‘GSVA’ package (*Hänzelmann, Castelo & Guinney, 2013*) in R to obtain the enrichment score of each patient. Each sample’s immune and stromal levels (immune score, stromal score, ESTIMATE score, and tumor purity) were obtained using an estimate algorithm (*Ke et al., 2020*). We performed 50 iterations of consistent clustering with a resample rate of 80% for each patient based on the immune cell infiltration (ICI) pattern using “ConsensusClusterPlus” package (*Wilkerson & Hayes, 2010*). We used the “pheatmap” package to visualize the clustering results. We designated the three clusters, ICICluster 1, ICICluster 2, and ICICluster 3, according to their ICI levels (from low to high).

ICI cluster differentially expressed gene (DEG) analysis

Considering that some of the samples had a gene expression level of 0 which would lead to bias in the results, we only selected genes with mean gene expression levels greater than or equal to 0.1 for use in the subsequent study. DEGs were screened and identified from the three ICI clusters using $|\text{Log}_2 \text{ fold change (LogFC)}| > 1.8$ and a false discovery rate (FDR) < 0.01 , which was implemented by the Wilcoxon test. Univariate COX analysis (*Tibshirani, 2009*) was used to determine the prognostic DEGs with $p < 0.01$.

Identifying gene clustering and ICIScore generation

Using the consistent clustering method, we identified three gene clusters. The genes that positively and negatively correlated with ICICluster were designated as the upregulated and downregulated genes, respectively. We used a principal-component analysis (PCA) algorithm (*Ringnér, 2008; David & Jacobs, 2014; Konishi et al., 2019*) to extract the first principal components of the upregulated and downregulated genes. Next, we defined the ICIScore of each patient:

$$\text{ICIScore} = \sum \text{PCA}_u - \sum \text{PCA}_d$$

where u refers to the upregulated genes and d refers to the downregulated genes.

We selected the best cutoff using the “survminer” package. According to the cutoff, we divided the patients into two groups (ICIScore low and ICIScore high).

Constructing the prognostic signature and Riskscore generation

We randomly divided TCGA patients into two cohorts. Cox proportional hazard models are the most widely-used approach for modeling time to event data. They use the principle of recursive elimination to compute the instantaneous rate of an event occurrence (Asano, Hirakawa & Hamada, 2014). We constructed a 5-mRNA prognostic signature using the COX-PH algorithm. Next, we defined the Riskscore (Lee, 2008) of each patient:

$$\text{Riskscore} = \sum_{i=1}^n \text{Exp}i \times \text{Coef}$$

where n refers to the number of genes in the signature, $\text{Exp}i$ refers to the level of gene expression in the signature, and Coef refers to the estimated regression coefficient value from the COX-PH algorithm. According to their Riskscore median, the patients were divided into two groups (Riskscore low and Riskscore high). The signature was also fitted in the testing set and the total set.

Statistical analysis

All statistical analyses were conducted using R (3.6.1) software. We used the Mann–Whitney U test to compare two groups, and the Kruskal–Wallis test to compare more than two groups. The Kaplan–Meier (K-M) survival curves (You et al., 2018) were used to generate different groups of DFS curves. The receiver operating characteristic curves (ROC) (Blangero et al., 2020) was used to identify the Riskscore prognosis. Two-tailed P values less than 0.05 were considered statistically significant.

RESULTS

The landscape of tumor-infiltrating immune cells

The detailed flow chart of this study is shown in Fig. 1. Using the gene set associated with 28 types of infiltrating immune cells (Table S1) (Charoentong et al., 2017) and the ssGSEA algorithm, we obtained the enrichment score of the tumor-infiltrating immune cells in each PTC sample. Using consistent clustering, we divided the PTC patients into three ICI subtypes (Fig. 2A and Fig. S1). Based on the correlation analysis, we generated a correlation matrix of the tumor-infiltrating immune cells (Fig. 2B). Almost all of the items showed a positive correlation. The most significant correlation was shown between Myeloid-derived suppressor cells (MDSC) and other cells, especially MDSCs and effector memory CD8 T cells (Khaled, Ammori & Elkord, 2013; Lechner et al., 2011). We used the Kruskal–Wallis test to compare the enrichment score across the three ICI subtypes (Fig. 2C) and we found that there were significant differences across the three ICI groups, indicating that our clustering was successful. Additionally, we performed pairwise combinations of the three ICI subtypes, and the Mann–Whitney U test to compare the expression levels of two immune checkpoint-related genes (PD-L1 and CTLA-4) in every combination (Figs. 2D and 2E). To explore the biological processes of the different ICI clusters, we used GSEA enrichment analysis (Subramanian et al., 2005) on the different ICI clusters. The ICI cluster 2 pathway was significantly enriched compared to ICI cluster 1

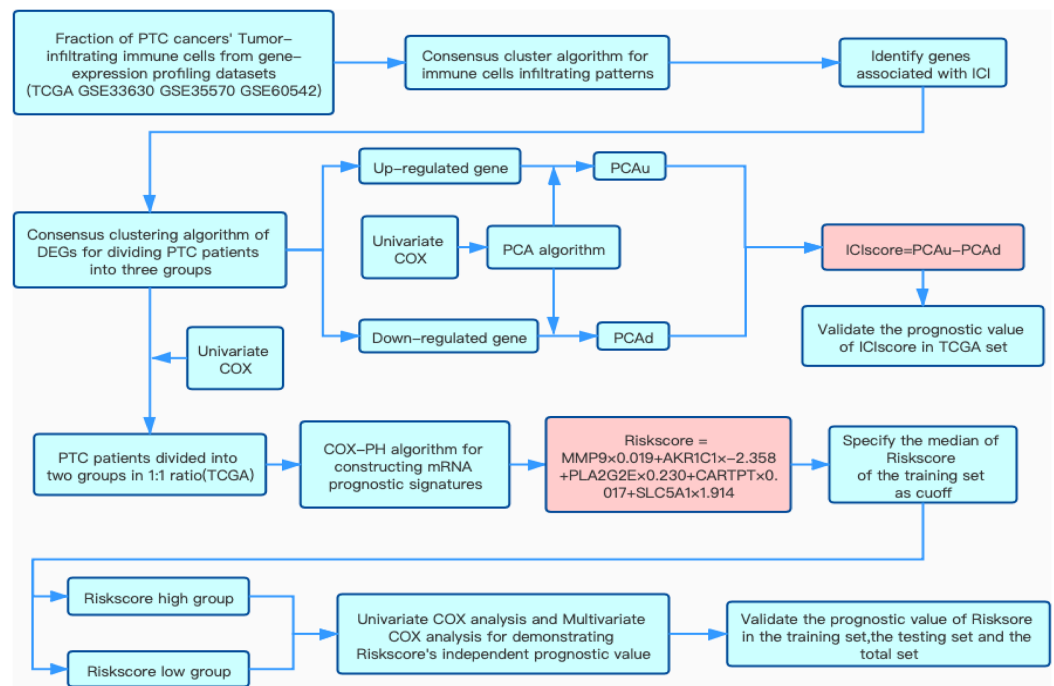


Figure 1 Flow chart of this study. Overview of research design

Full-size DOI: 10.7717/peerj.11494/fig-1

(Fig. 3A). Similarly, Fig. 3B shows that the ICIcluster 3 pathway was significantly enriched compared to ICIcluster 2. Detailed enrichment results can be seen in Table S2.

The same approach was applied to the GEO combined sets. We used consistency clustering to divide patients into three groups (Fig. S2A). The correlation analysis of the 28 types of tumor-infiltrating immune cells is shown in Fig. S2B. Significant differences were shown across the three ICIclusters (Fig. S2C), which was consistent with the performance of TCGA set. In the analysis of the immune checkpoint-related genes (PD-L1 and CTLA-4), there were also significant differences across the ICIclusters (Figs. S2D–S2F). GSEA enrichment analysis was also performed for the different ICIclusters, and the results can be found in Figs. S3A and S3B. Detailed enrichment results can be seen in Table S3. In the most significant Top 10 enrichment pathway, the GEO combined set and TCGA set were consistent with one another. This suggests that our ICIclusters represented the tumor-infiltrating immune cell landscape of PTC patients and will lay the foundation for subsequent analysis.

Stratified DFS analysis of the three ICI subtypes

The three ICI subtypes showed different DFS conditions compared to the total set (Fig. 3C). ICIcluster 3 had the most significant immune cell infiltration and was associated with the best prognosis. It is notable that ICIcluster 2 showed moderate immune cell infiltration but was associated with the worst prognosis. Although ICIcluster 1 had the lowest immune cell infiltration, it was associated with a moderate prognosis. Such results were also reflected in the Age <45 and T3 + T4 groups (Fig. 3D). This indicates that high or

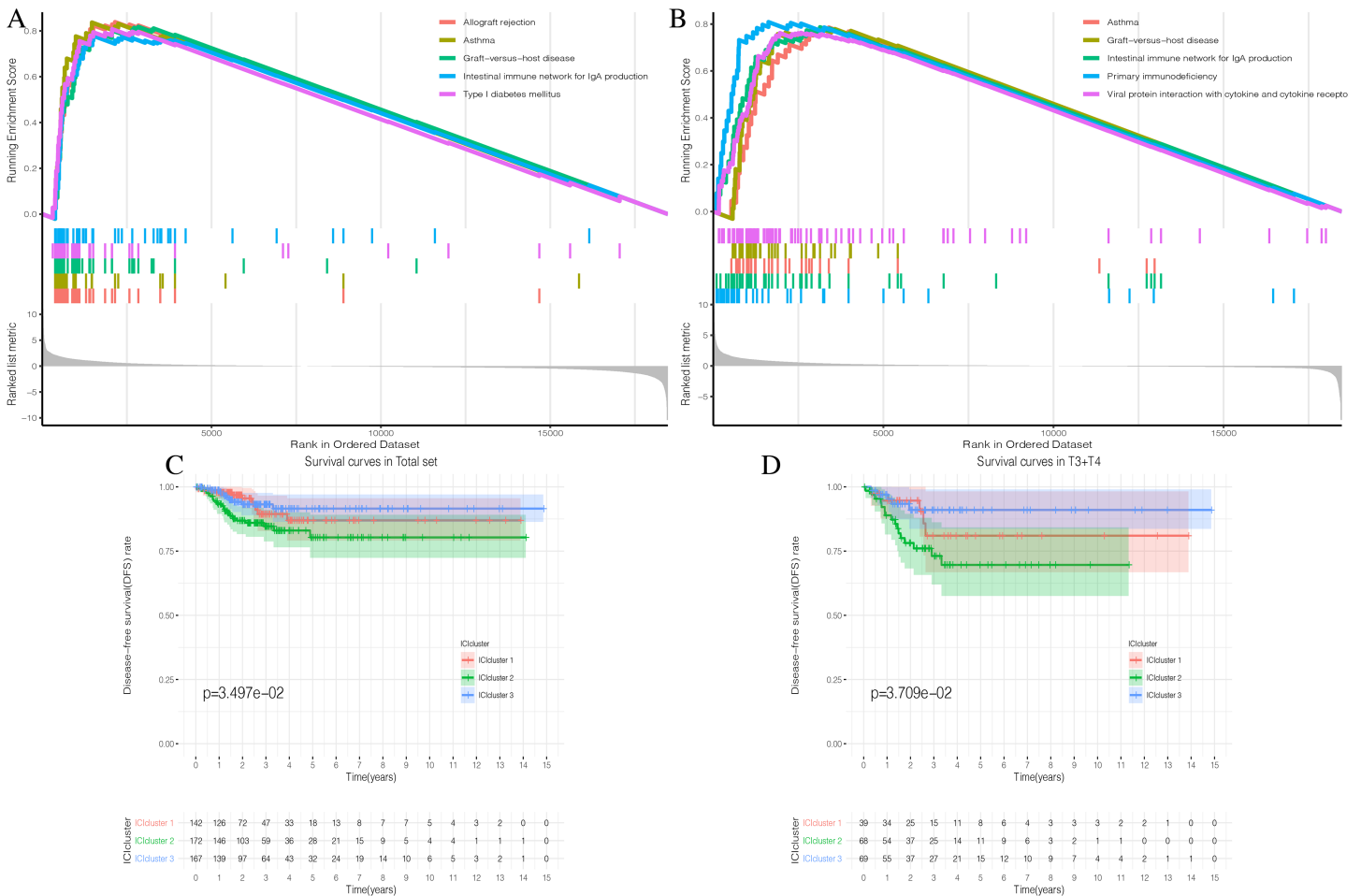


Figure 3 Prognostic correlation analysis of three ICi clusters. (A and B) Enrichment plots showing different enrichment of different diseases and pathways in the Rank in Ordered Dataset. (C) The Kaplan-Meier (K-M) curves of Disease-free survival (DFS) in Total set (D) The Kaplan-Meier (K-M) curves of Disease-free survival (DFS) in T3 + T4
Full-size [DOI: 10.7717/peerj.11494/fig-3](https://doi.org/10.7717/peerj.11494/fig-3)

subtypes. We used the Wilcoxon-test to identify the DEGs associated with the three ICI subtypes. With $|\text{LogFC} > 1.8|$ and $\text{FDR} < 0.01$, we obtained 982 DEGs: 752 upregulated genes and 230 downregulated genes (Fig. S4, Table S4). Upregulated genes were those that were highly expressed in at least two ICI subtypes with higher immune cell infiltration. The rest were labeled downregulated genes. To determine the underlying biological functions of the DEGs, we conducted Gene Ontology (GO) and Kyoto Encyclopedia of Genes and Genomes (KEGG) enrichment analyses (Xing et al., 2020; Wang et al., 2020) of the upregulated genes and downregulated genes, respectively. The most significant enrichment results are summarized in Figs. 4A–4D, and detailed content is provided in Table S5. Using $P < 0.01$ as the cutoff, we performed univariate COX analysis to identify the DEGs associated with prognosis. Finally, we obtained 15 DEGs: 10 upregulated and five downregulated genes (Table 1).

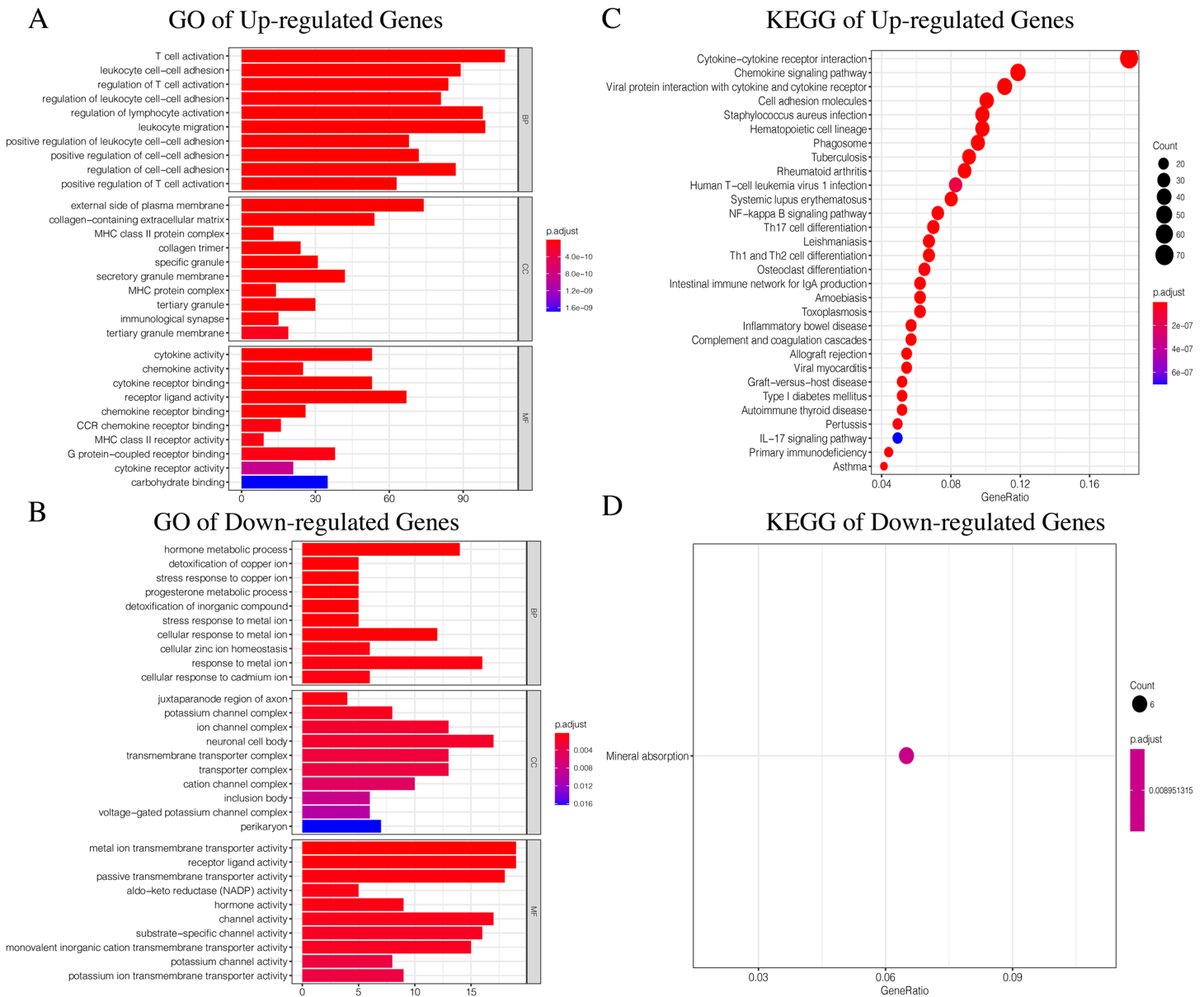


Figure 4 The GO and KEGG enrichment analysis of Up-regulated Gene and Down-regulated Gene. (A) The GO enrichment analysis of Up-regulated Gene. (B) The GO enrichment analysis of Down-regulated Gene. (C) The KEGG enrichment analysis of Up-regulated Gene. (D) The KEGG enrichment analysis of Down-regulated Gene. [Full-size !\[\]\(5fd6ef84f97f42d7f8b34275f1b65312_img.jpg\) DOI: 10.7717/peerj.11494/fig-4](https://doi.org/10.7717/peerj.11494/fig-4)

Identifying immune gene subtypes

Using our consistent cluster analysis of the 15 genes listed above, we obtained three gene clusters (Fig. 5A). In order to explore the abundance of immune cell infiltration across the three gene subtypes, we performed Kruskal–Wallis tests on the three subtypes.

We found that Genecluster 1 and Genecluster 3 had more tumor-infiltrating immune cells and that Genecluster 3 was more significant than Genecluster 1 (Fig. 5B). This difference at the immune level was also shown in the expression levels of the two immune checkpoint-related genes (PD-L1 and CTLA-4; Figs. 5C–5D). Furthermore, we also

Table 1 Univariate COX analysis of differentially expressed gene.

Symbol	Entrez ID	HR	95% CI		P value	Gene type
			Low	High		
AKR1C1	1645	0.068	0.010	0.437	0.005	Down-regulated Gene
MYH3	4621	1.109	1.060	1.159	<0.001	Down-regulated Gene
CSMD1	64478	1.239	1.117	1.374	<0.001	Down-regulated Gene
CARTPT	9607	1.003	1.001	1.005	0.003	Down-regulated Gene
SLC5A1	6523	1.222	1.069	1.396	0.003	Down-regulated Gene
MMP9	4318	1.012	1.003	1.021	0.010	Up-regulated Gene
FN1	2335	1.000	1.000	1.001	<0.001	Up-regulated Gene
PLA2G2E	30814	1.231	1.107	1.369	<0.001	Up-regulated Gene
C2CD4A	145741	1.108	1.051	1.169	<0.001	Up-regulated Gene
DAW1	164781	3.126	1.322	7.395	<0.001	Up-regulated Gene
MUC21	394263	1.026	1.009	1.042	0.002	Up-regulated Gene
AHNAK2	113146	1.054	1.017	1.093	0.004	Up-regulated Gene
IL1RN	3557	1.062	1.024	1.101	0.001	Up-regulated Gene
DCSTAMP	81501	1.007	1.002	1.013	0.005	Up-regulated Gene
SLC34A2	10568	1.001	1.000	1.001	0.008	Up-regulated Gene

Note:

HR, hazard ratio; CI, confidence interval.

explored the prognostic differences across the three gene subtypes. Genecluster 1 and 2 were associated with a favorable prognosis while Genecluster 3 was associated with the worst prognosis (Fig. 6A). It is worth noting that in addition to the worst prognosis, Genecluster 3 also had the most immune infiltrating cells. The immune system's specific mechanism involved with tumor occurrence and development is worthy of further investigation, as its activation may have both favorable and unfavorable results. According to clinical stratification studies, similar results can also be seen in patients who were female, age <45, age >45, N1, Stage I + Stage II, and T1 + T2 (Figs. 6B–6G).

Generation and validation of the ICIScore groups

We used the PCA algorithm to calculate the ICIScore for each PTC sample. The ICIScore consisted of two parts: (1) the PCAu calculated from upregulated genes and (2) the PCAd calculated from downregulated genes. The PCAu and PCAd of each sample were the first principal components of the relevant gene. Finally, using the ICIScore formula, we obtained the ICIScore of each sample. With the “survminer” package, we calculated the optimal ICIScore cutoff as 2.17 (Fig. 7A) and divided the patients into two groups (ICIScore high and ICIScore low). Since the ICIScore correlated with immune status and the immune score reflected the level of immune cell infiltration, it was reasonable to believe that there was a correlation between these values. In order to explore this relationship, we drew a scatter plot (Fig. 7B) that showed a highly positive correlation between the two, indicating that ICIScores could reflect the level of immune cell infiltration to some extent. Although immune scores do not have prognostic value, we found that ICIScores did correlate with prognosis in a follow-up study. The distribution of all patients is shown in

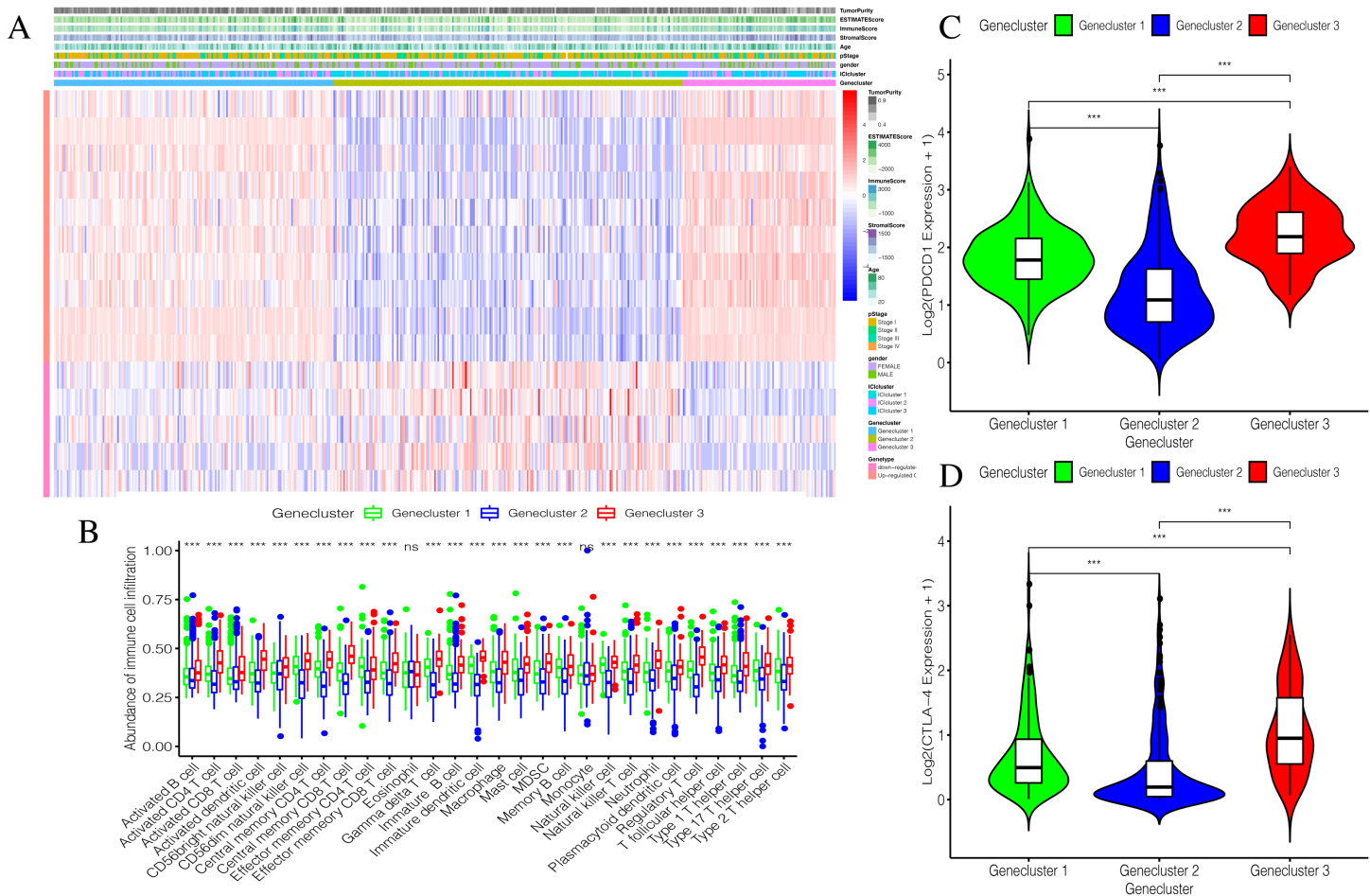


Figure 5 Establishment and verification of Geneclusters. (A) The heat map is included the tumor purity, estimate score, immune score, stromal score, age, pStage, gender, ICIcluster and Genecluster. (B) Comparison of infiltration levels of immune cells in three Geneclusters. (C) The expression level of immune checkpoint related gene PD-L1. (D) The expression level of immune checkpoint related gene CTLA4.

Full-size DOI: 10.7717/peerj.11494/fig-5

Fig. 7C. Patients with high ICIscores were mainly distributed in Genecluster 3 with poor prognosis predicted. To determine whether different ICIscore groups had different prognoses, we plotted the K-M survival curve. We found that the ICIscore high group showed significantly poorer prognoses (Fig. 7D). To evaluate whether ICIscores reflected differences in immune levels across the groups, we compared the tumor-infiltrating immune cells between the two groups using a Mann-Whitney U test (Fig. 7E). Additionally, we selected PDCD1, CD274, CTLA-4, LAG3, and IDO1 as the immune checkpoint-related genes and IL1A, IL1B, IL6, IL8, IFNG, and TNF as the immune active factors (Ayers et al., 2017; Deng et al., 2012). The Mann-Whitney U test showed that most immune checkpoint-related genes, except PDCD1 and TNF, and immune active factors were highly expressed in the ICIscore high group (Fig. 7F). Based on the GSEA results, we also found that the “allograft rejection” and “graft-versus-host disease” pathways were significantly enriched in the ICIscore high group, while the “maturity onset diabetes of the

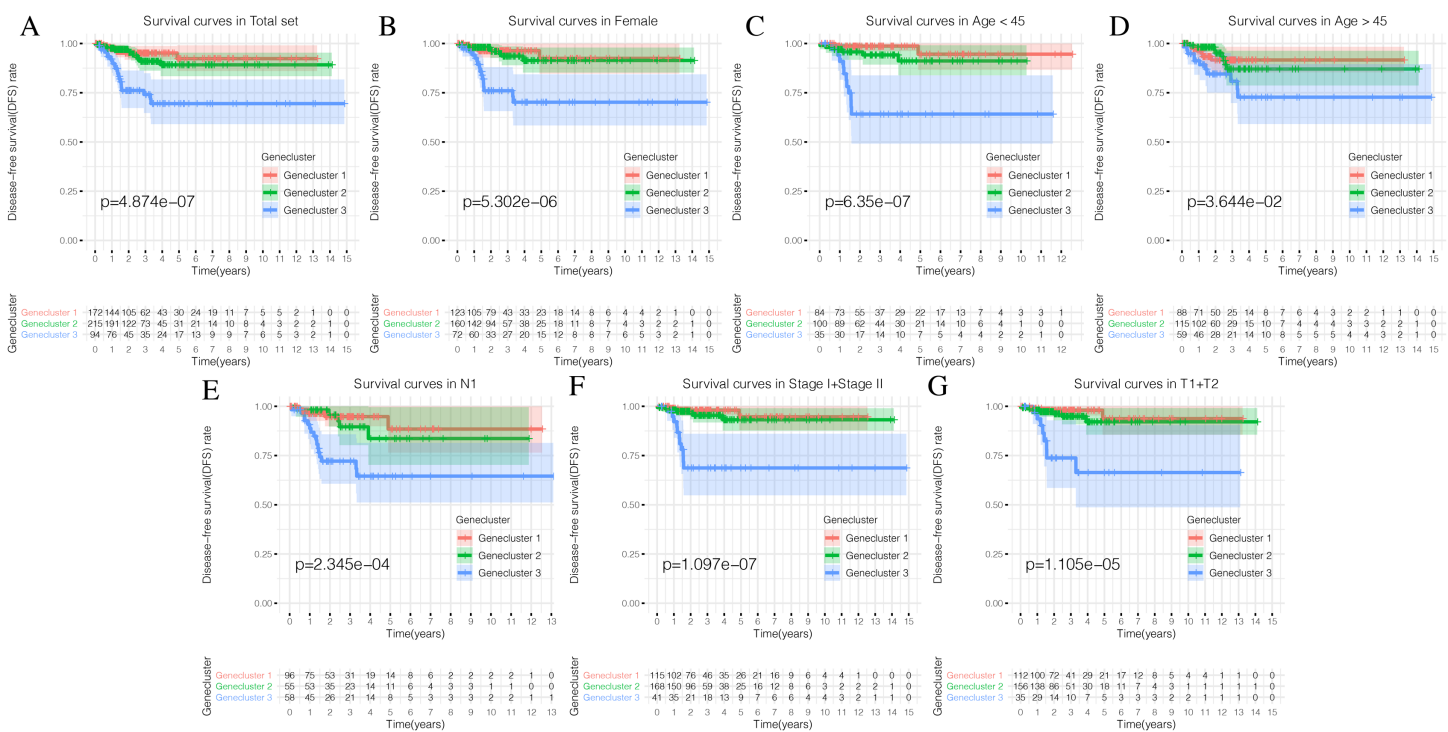


Figure 6 Prognostic differences of the three Geneclusters. (A) The Kaplan-Meier (K-M) curves of Disease-free survival (DFS) in total set. (B) The Kaplan-Meier (K-M) curves of Disease-free survival (DFS) in female. (C) The Kaplan-Meier (K-M) curves of Disease-free survival (DFS) in age <45. (D) The Kaplan-Meier (K-M) curves of Disease-free survival (DFS) in age >45. (E) The Kaplan-Meier (K-M) curves of Disease-free survival (DFS) in N1. (F) The Kaplan-Meier (K-M) curves of Disease-free survival (DFS) in Stage1 + Stage2. (G) The Kaplan-Meier (K-M) curves of Disease-free survival (DFS) in T1 + T2. Full-size [DOI: 10.7717/peerj.11494/fig-6](https://doi.org/10.7717/peerj.11494/fig-6)

young” and “olfactory transduction” pathways were significantly enriched in the ICIScore low group (Figs. 7G–7H, Table S6).

Generation and validation of the Riskscore group

To further explore the potential prognostic value of these genes, we randomly divided TCGA PTC patients into two groups at a 1:1 ratio. We used the COX-PH algorithm to construct a 5-mRNA prognostic signature (Fig. 8A, Table 2). We specified the Riskscore median cutoff of the training set to fit the testing set and the total set. $\text{Riskscore} = \text{MMP9} \times 0.019 + \text{AKR1C1} \times -2.358 + \text{PLA2G2E} \times 0.230 + \text{CARTPT} \times 0.017 + \text{SLC5A1} \times 1.914$. Previous literature suggested that these five genes were closely related to cancer prognosis. In addition, it has been reported that the elevated MMP-9 level in PTC patients is defined as a malignant factor of PTC (Zarkesh et al., 2018) and may be involved in the mechanism of ROCK1 in the occurrence and development of PTC (Luo et al., 2017). AKR1C1, PLA2G2E, CARTPT, and SLC5A1 have been shown to be abnormally expressed in cancer and influence prognosis (Zeng et al., 2017; Sato et al., 2014; Burgos, Iresjö & Smedh, 2016; Gao et al., 2019; Mojica, Luna-Vital & Gonzalez de Mejia, 2018; Lei et al., 2016).

The distribution of all patients is shown in Fig. 8B. Patients with high Riskscores had poor prognosis. Before verifying the signature’s prognostic effect, we compared the immune cell infiltration between the two Riskscore groups (Fig. 8C). There was a

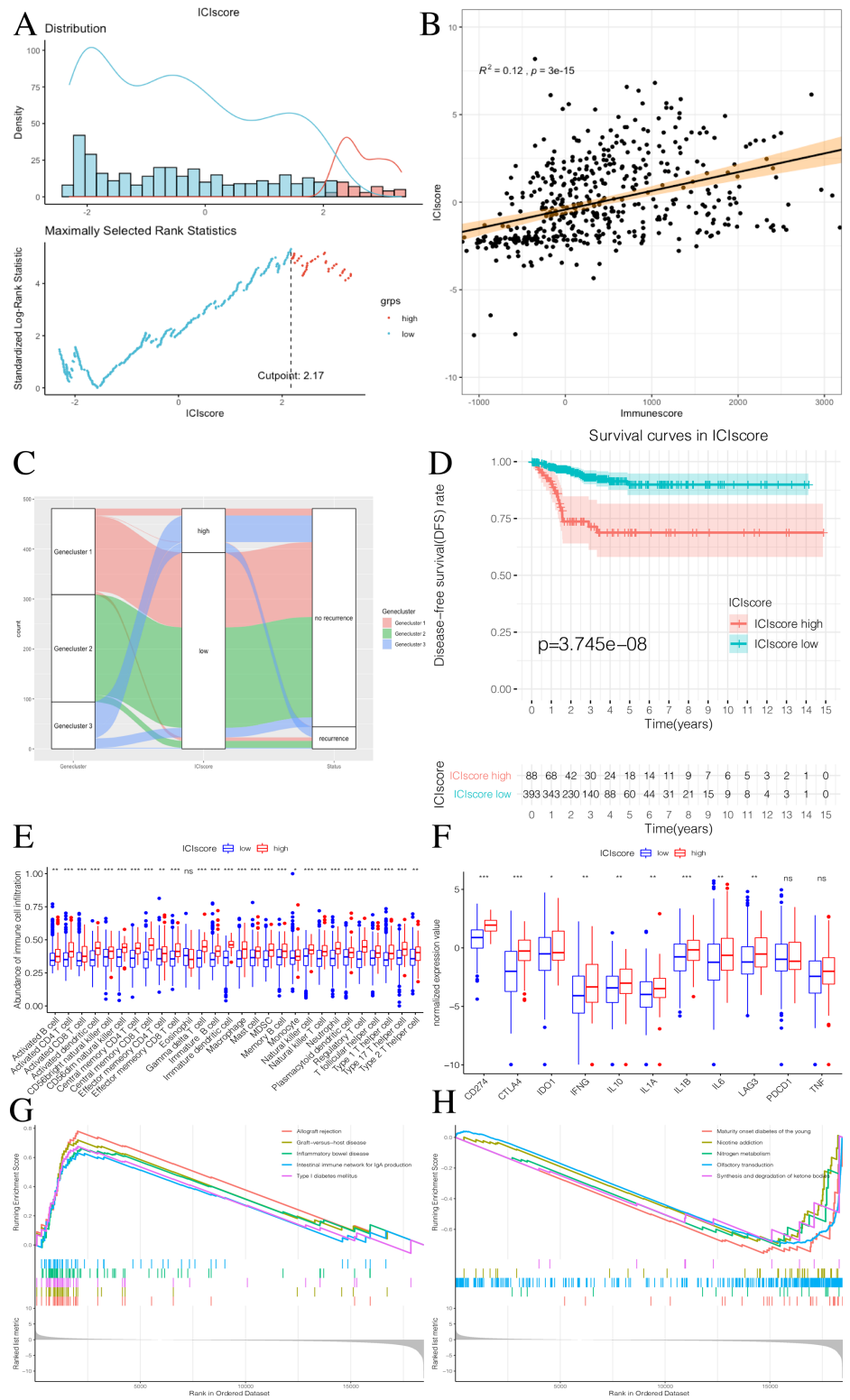


Figure 7 Construction of ICI score and its clinical prognostic analysis. (A) The construction of ICI score with high and low grouping model. (B) The scatter plot showing the relationship between ICI score and Immunescore. (C) Alluvial diagram of Genecluster distribution in groups with different Geneclusters, ICI scores, and survival outcomes. (D) The Kaplan-Meier (K-M) survival curves in ICI score

Figure 7 (continued)

high and low grouping. (E) Differences in immune cell infiltration expressed in high and low ICI score subgroups. (F) Immune-checkpoint-relevant genes and immune-activation-relevant genes expressed in high and low ICI score subgroups. (G and H) Enrichment plots showing different enrichment of different pathways in the ICI score high and low grouping. [Full-size !\[\]\(c3cffc168beb4396c1e1a5a6db5d66b0_img.jpg\) DOI: 10.7717/peerj.11494/fig-7](https://doi.org/10.7717/peerj.11494/fig-7)

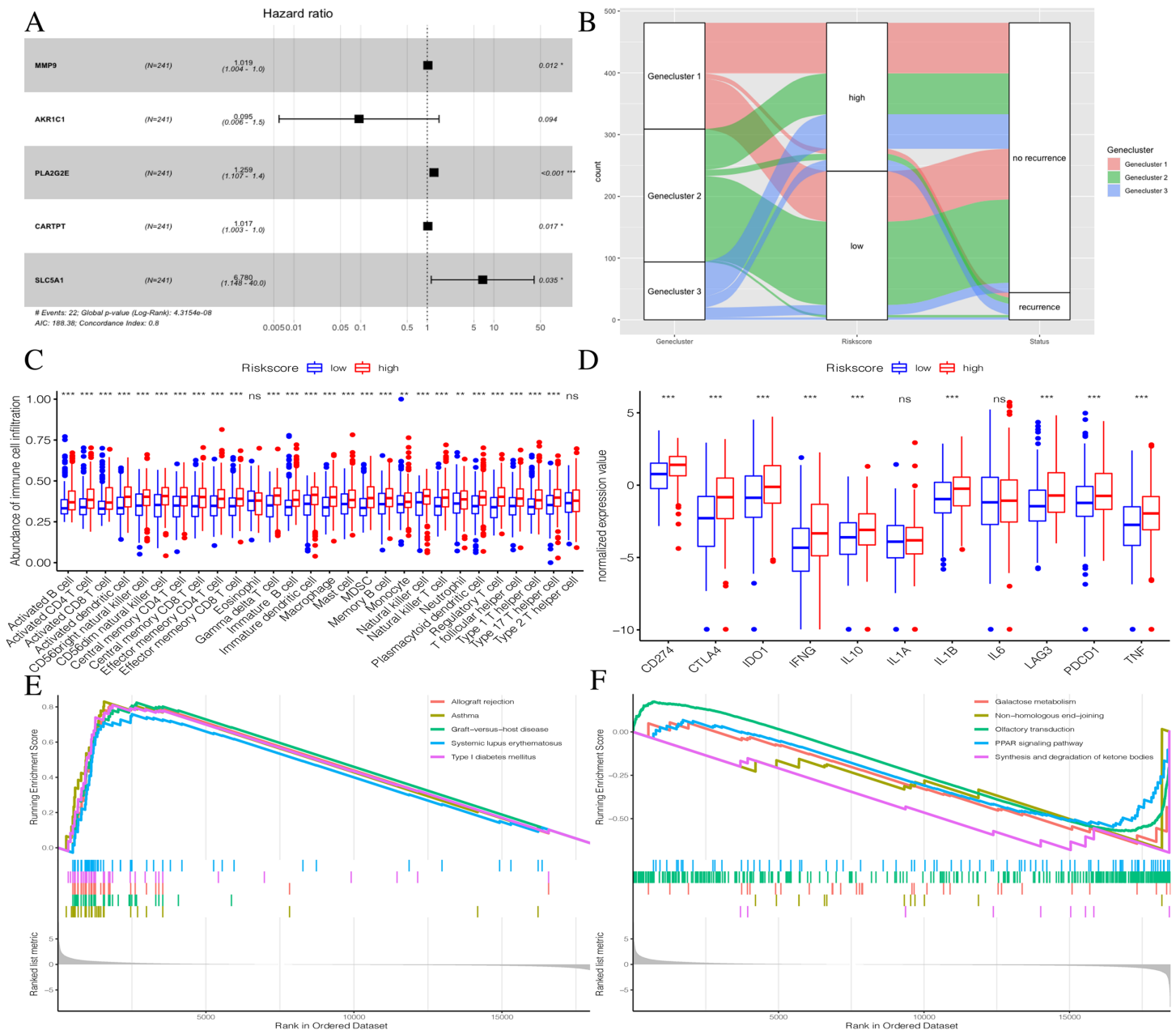


Figure 8 Construction of Riskscore. (A) The construction of a 5-mRNA prognostic signature. (B) Alluvial diagram of Genecluster distribution in groups with different gene clusters, risk, and Disease-free survival (DFS) outcomes. (C) Differences in immune cell infiltration expressed in high and low Riskscore. (D) Immune-checkpoint-relevant genes and immune-activation-relevant genes expressed in high and low Riskscore. (E and F) Enrichment plots showing different enrichment of different pathways in the Riskscore high and Riskscore low. [Full-size !\[\]\(7b16a8a038e480c725c91707e7077853_img.jpg\) DOI: 10.7717/peerj.11494/fig-8](https://doi.org/10.7717/peerj.11494/fig-8)

Table 2 COX-PH algorithm constructed 5-mRNA signature.

Symbol	Coef	HR	95% CI		P value
			Low	High	
MMP9	0.019	1.019	1.004	1.034	0.012
AKR1C1	-2.358	0.095	0.006	1.497	0.094
PLA2G2E	0.230	1.259	1.107	1.431	<0.001
CARTPT	0.017	1.017	1.003	1.032	0.017
SLC5A1	1.914	6.780	1.148	40.034	0.035

Note:

Coef, Coefficient of the model; HR, hazard ratio; CI, confidence interval.

significant difference in the level of immune cell infiltration between the two groups, and the Riskscore high group showed more immune cell infiltration. Additionally, most immune checkpoint-related genes and immune active factors, except IL1A and IL6, were highly expressed in the Riskscore high group (Fig. 8D). We also performed GSEA enrichment analysis on the two groups. The “allograft rejection” and “asthma” pathways were significantly enriched in the Riskscore high group, while the “synthesis and degradation of ketone bodies” and “on-homologous and end-joining” pathways were significantly enriched in the Riskscore low group (Figs. 8E and 8F). More details are shown in Table S7.

By plotting K-M survival curves for the training, testing, and the total sets, we found that the Riskscore high group had a significantly poor prognosis (Figs. 9A–9C). In order to reveal the prognostic value of the signature, we verified the prognostic Riskscore value by drawing ROC curves for the different time periods (1-year, 3-years, and 5-years; Figs. 9D–9F). The AUC of the training, testing, and total set were mostly greater than 0.7, indicating that our signature had good prognostic value.

ICIscore and Riskscore clinical correlation analysis

While exploring potential independent prognostic factors, we did not include pM stages in this study due to the presence of many missing values in pM stages. Using univariate and multivariate COX analysis, we found that ICIscores and Riskscores could be used as independent prognostic factors (Figs. 10A–10D). Additionally, pT, pN, and pStage may also be potential prognostic factors according to univariate COX analysis with P value < 0.05. The nomograms showed the different clinical traits of patients without scores, with ICIscore or with Riskscore (Figs. 10E–10G). This provides a clinical reference for these patients' prognosis.

DISCUSSION

Immune cells play an important role in tumor prevention, initiation, and progression (Crespo et al., 2013). The majority of PTC patients have excellent prognoses, but there are patients who experience disease recurrence and progression. Therefore, it is necessary to analyze the prognosis of all PTC patients.

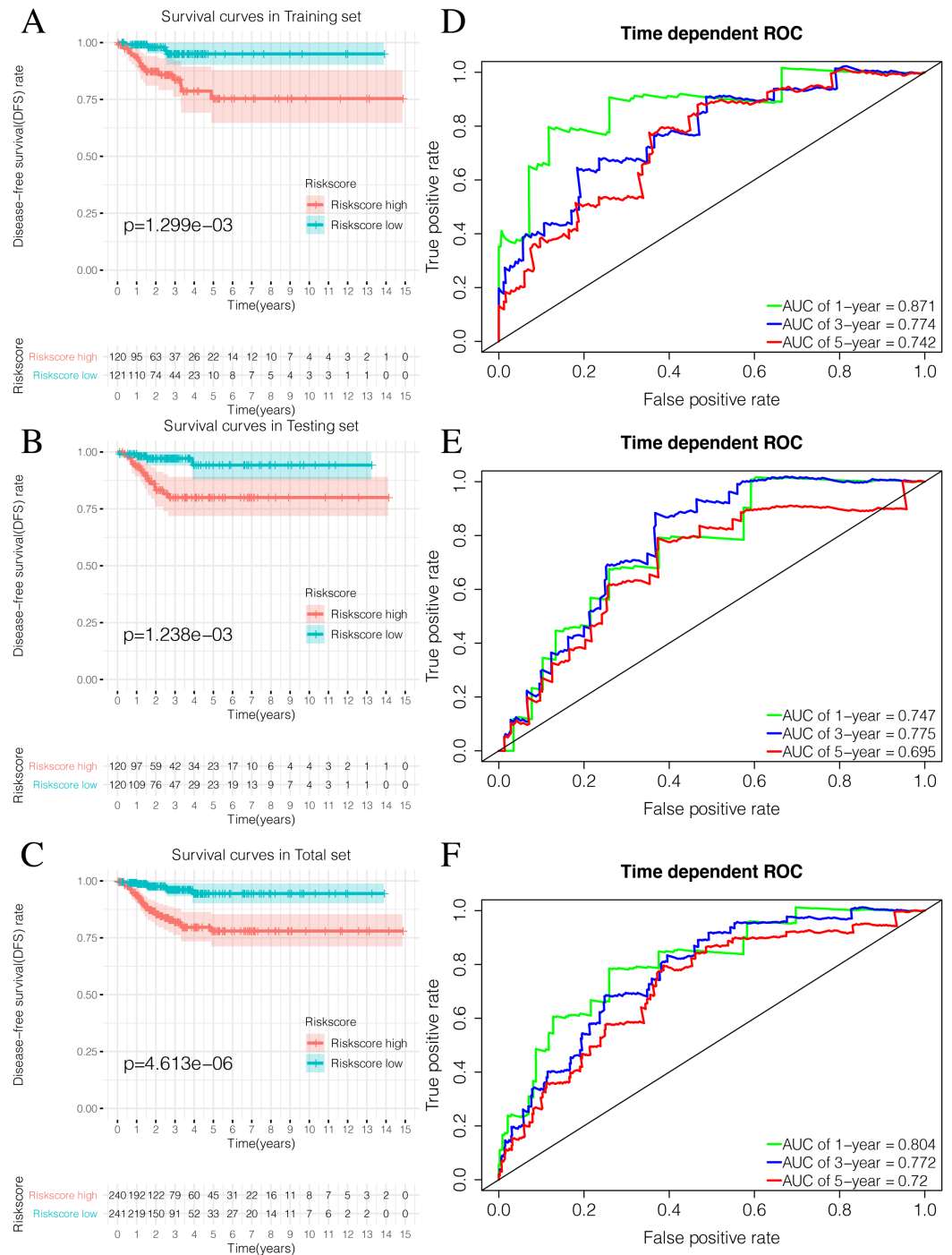


Figure 9 Validation of the prognostic signature of Riskscore. (A) The Kaplan-Meier (K-M) curves of Disease-free survival (DFS) in the training set. (B) The Kaplan-Meier (K-M) curves of Disease-free survival (DFS) in the testing set. (C) The Kaplan-Meier (K-M) curves of Disease-free survival (DFS) in the total set. (D-F) Time-dependent ROC curves in the training set, testing set and the total set at 1-year, 3-year and 5-year. [Full-size !\[\]\(ebfe6d37ad86655679811e032f633da4_img.jpg\) DOI: 10.7717/peerj.11494/fig-9](https://doi.org/10.7717/peerj.11494/fig-9)

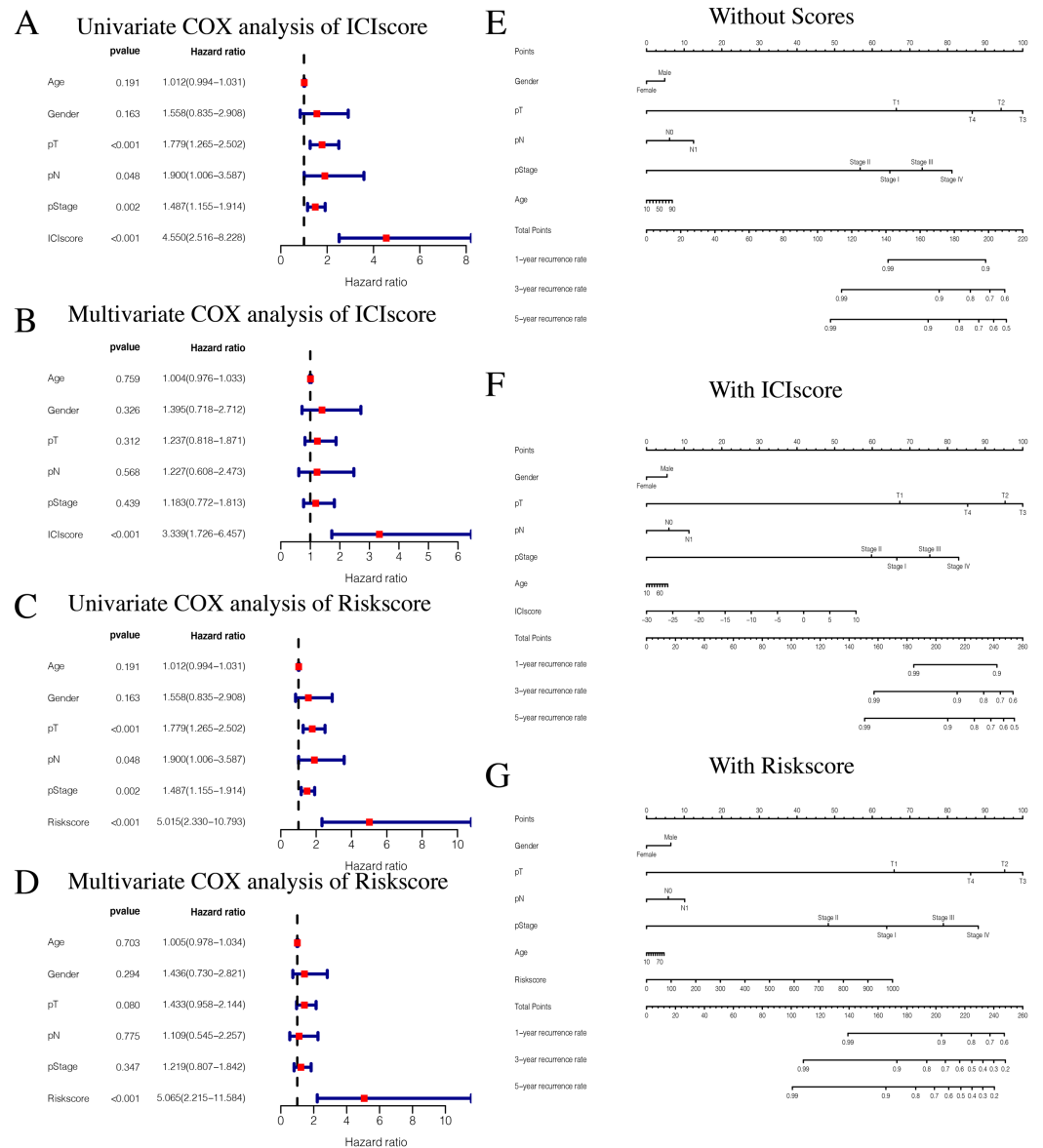


Figure 10 Independent prognostic analysis of ICI score and RiskScore. (A) Univariate COX analysis of ICI score about PTC prognostic signatures and clinical characteristics. (B) Multivariate COX analysis of ICI score about PTC prognostic signatures and clinical characteristics. (C) Univariate COX analysis of RiskScore about PTC prognostic signatures and clinical characteristics. (D) Multivariate COX analysis of RiskScore about PTC prognostic signatures and clinical characteristics. (E) The nomogram of different clinical traits of the patients without scores. (F) The nomogram of different clinical traits of the patients with ICI score. (G) The nomogram of different clinical traits of the patients with RiskScore.

Full-size [DOI: 10.7717/peerj.11494/fig-10](https://doi.org/10.7717/peerj.11494/fig-10)

We first obtained clinical data from 481 PTC patients with effective DFS time from TCGA database. Using the ssGSEA algorithm, we obtained enrichment scores for the tumor-infiltrating immune cells in each PTC sample. The PTC patients were divided into three ICI subtypes using consistent clustering. The results showed that almost all items were positively correlated, and that the most significant correlation was observed between

MDSCs and other cells, particularly between MDSCs and effector memory CD8T cells. MDSCs are a subset of functional myeloid cells with immunosuppressive properties. They are the precursor of dendritic cells (DCs) and macrophages and/or granulocytes, and they have the ability to significantly inhibit the immune cell response. MDSCs exert immunosuppressive functions through a variety of pathways and mechanisms, and can suppress lymphocytes by secreting Arg-1, iNOS, or ROS. Additionally, Treg can also be induced to indirectly inhibit the body's immune response. MDSCs have been found in the peripheral blood of patients with several malignant and non-malignant diseases. They are produced during tumor progression and inhibit the antitumor function of T cells and natural killer cells (NK cells). Their abundance is associated with poor prognosis in cancer patients and poor immunotherapy outcomes (Weber *et al.*, 2021). MDSCs have strong immunosuppressive potential and are an important component of the tumor microenvironment (TME). Tumor cells use MDSC inhibition mechanism to establish immunosuppressive TME, thereby inhibiting anti-tumor immune responses and promoting tumor progression (Kalathil & Thanavala, 2021). Our data further confirm the role of MDSCs as cancer surveillance tools. We compared the enrichment scores across the ICI subtypes, and the results showed that there were significant differences across the three ICI groups, indicating that our clustering would be valuable and instructive in clinical practice. Because ICIcluster 3 had the highest level of immune cell infiltration, we inferred that a high level of immune cell infiltration could be associated with the best prognosis. Notably, ICIcluster 2 showed moderate immune cell infiltration but was associated with the worst prognosis, while ICIcluster 1 had the lowest level of immune cell infiltration but was associated with a moderate prognosis. Considering that there may be potential molecular differences across different ICI subtypes, we screened out DEGs associated with the three ICI subtypes. Upregulated genes were defined as being highly expressed in at least two ICI subtypes with higher immune cells. We ultimately obtained 15 differentially expressed genes: 10 upregulated genes and five downregulated genes.

Through our consistent cluster analysis of the above 15 genes, we obtained three gene clusters. The immune cell infiltration levels showed that Genecluster 1 and Genecluster 3 had more tumor-infiltrating immune cells, and Genecluster 3 was more significant than Genecluster 1.

Additionally, prognostic differences across the three gene clusters were explored. Genecluster 1 and Genecluster 2 showed better prognoses, while Genecluster 3 was associated with the worst prognosis. However, in combination with previous results, Genecluster 3 had more immune-infiltrating cells, but had the worst prognosis. The role of the immune system in the development of cancer is worth further study, as its activation may have both positive and negative consequences. Both high and low immunity can promote tumor occurrence and development. The association between high immune levels and tumors may be related to an increase in immune escape. Researchers have studied the immune system's reactivation when fighting cancer since the end of the 19th century. Cooley was the first to demonstrate that bacterial infections induced in cancer patients could eliminate, or at least slow down, the disease (Zhao *et al.*, 2020). After several decades, the seminal work of the two 2018 Nobel Prize in Medicine winners, James Patrick Allison

and Tasuku Honjo, further validated the use of immune checkpoint inhibitors in cancer treatment (Coley, 1991). Because of these findings, many immune checkpoint inhibitors have received FDA approval for cancer treatment. It could be said that suppressing the level of immune cell infiltration to treat cancer is now a universally accepted fact. However, some studies have shown that low levels of immune cell infiltration are associated with a better cancer prognosis (Aaes & Vandenabeele, 2020). This opposing conclusion suggests that the immune system has two functions during tumor development. Therefore, it is necessary to further study the effect of immune cell infiltration levels on tumors.

According to the results described above, the ICIScore and Riskscore immune infiltration levels were highly consistent, suggesting similarities across most of the pathways enriched by GSEA. This was also shown in previous research by Subramanian *et al.* (2005).

We calculated ICIScores for each PTC sample and used the optimal ICIScore cutoff value in order to divide the patients into two groups (high ICIScore and low ICIScore). The results showed that patients with high ICIScores were mainly distributed in Genecluster 3 with poor predicted prognoses. In order to verify whether ICIScores were related to differences in immune levels between the two groups, we compared the tumor-infiltrated immune cells between the two groups using the Mann–Whitney *U* test. We also selected some immune checkpoint-related genes and immunoactive factors. The Mann–Whitney *U* test showed that, except for PDCD1 and TNF, most of the immune checkpoint-related genes and immune active factors were highly expressed in the ICIScore high group (Leach, Krummel & Allison, 1996). This again demonstrated the association between high immunity and poor prognosis.

To further explore the potential prognostic value of the genes, we constructed the prognostic characteristics of five mRNA. Studies have shown that MMP9 is associated with KDM1A and Inava. KDM1A can apparently inhibit the expression of TIMP1 by demethylating H3K4ME2 in the TIMP1 promoter region, activating MMP9, which is responsible for tumor migration and PTC invasion through this pathway (Zhang *et al.*, 2019). The expression levels of AKR1C1 family members is strongly correlated with the malignant transformation of tumors and drug resistance to tumor therapy (Zeng *et al.*, 2017). PLA2G2E is mainly related with obesity. It changes small amounts of lipoprotein phospholipids, phosphatidylserine, and phosphatidylethanolamine to moderately promote lipid accumulation in liver and adipose tissue (Sato *et al.*, 2014). CARTPT is correlated with the neuroendocrine function of the hypothalamus, and may affect TSH levels (Burgos, Iresjö & Smedh, 2016). SLC5A1 plays a role in transmembrane glucose transport and encodes SGLT1. Abnormal SLC5A1 expression has been observed in many different types of cancer (Gao *et al.*, 2019; Mojica, Luna-Vital & Gonzalez de Mejia, 2018; Lei *et al.*, 2016).

We specified the median Riskscore value of the training set as the cut off and fit in the testing set and total set. There were significant differences in the infiltration levels of immune cells between the two groups, and the group with high Riskscore showed more immune cell infiltration. Additionally, most of the checkpoint-related genes and immune

activity factors, except IL1A and IL6, were highly expressed in the Riskscore high group. This suggests that immune system activation may be both harmful and beneficial to cancer prognosis, which is consistent with previous research (*Leach, Krummel & Allison, 1996*).

We constructed ICIscore and Riskscore signatures using a PCA algorithm and COX-PH algorithm, respectively. However, the advantages and disadvantages of these two algorithms are still worth exploring and comparing.

When combined with the above two models, the ICIscore *p*-value was smaller, suggesting that ICIscores may be more accurate in predicting the prognosis of PTC patients, and Riskscores may be more suitable for most PTC patients. We concluded that combining these two scoring mechanisms could effectively provide patients with more accurate prognostic analyses. Our results show a direction for individualized clinical treatment of PTC patients in the future. Nevertheless, there are still limitations to our study. Since the TCGA database was the only databases that includes disease-free survival and recurrence time of PTC, we could not verify the results externally. Therefore, the results of our study need to be supported by a large number of clinical data.

CONCLUSION

The results of this study showed that by combining the two constructed models, ICIscore and Riskscore, we made more accurate and reasonable inferences about the prognosis of PTC patients. This could potentially guide more effective and reasonable treatment plans for clinical PTC patients.

ACKNOWLEDGEMENTS

The authors would like to thank all the researchers who support the Cancer Genome Atlas and the Gene Expression Omnibus Research Network.

ABBREVIATIONS

PTC	Papillary thyroid carcinoma
ICI	Immune cell infiltration
DFS	disease-free survival
ssGSEA	Single Sample Gene Set Enrichment Analysis
CTLA-4	Cytotoxic T-lymphocyte antigen 4
PD-L1	Programmed cell death-Ligand 1
LogFC	Log2 fold change
FDR	false discovery
PCA	principal-component analysis
K-M curve	Kaplan-Meier curve
ROC	receiver operating characteristic curves
GO	Gene Ontology
KEGG	Kyoto Encyclopedia of Genes and Genomes

ADDITIONAL INFORMATION AND DECLARATIONS

Funding

This work was supported by The Youth Fund Project of Jiangxi Provincial Education Department (GJJ180146). The funders had no role in study design, data collection and analysis, decision to publish, or preparation of the manuscript.

Grant Disclosures

The following grant information was disclosed by the authors:

The Youth Fund Project of Jiangxi Provincial Education Department: GJJ180146.

Competing Interests

The authors declare that they have no competing interests.

Author Contributions

- Yanyi Huang conceived and designed the experiments, performed the experiments, analyzed the data, authored or reviewed drafts of the paper, and approved the final draft.
- Tao Yi conceived and designed the experiments, performed the experiments, analyzed the data, authored or reviewed drafts of the paper, and approved the final draft.
- Yushu Liu performed the experiments, analyzed the data, prepared figures and/or tables, and approved the final draft.
- Mengyun Yan analyzed the data, prepared figures and/or tables, authored or reviewed drafts of the paper, and approved the final draft.
- Xinli Peng performed the experiments, authored or reviewed drafts of the paper, and approved the final draft.
- Yunxia Lv conceived and designed the experiments, performed the experiments, analyzed the data, prepared figures and/or tables, authored or reviewed drafts of the paper, and approved the final draft.

Data Availability

The following information was supplied regarding data availability:

The raw data are available at TCGA (TCGA-THCA) and GenBank: [GSE33630](#), [GSE35570](#), [GSE60542](#).

Supplemental Information

Supplemental information for this article can be found online at <http://dx.doi.org/10.7717/peerj.11494#supplemental-information>.

REFERENCES

- Aaes TL, Vandenabeele P. 2020. The intrinsic immunogenic properties of cancer cell lines, immunogenic cell death, and how these influence host antitumor immune responses. *Cell Death and Differentiation* **28(843)**:860 DOI [10.1038/s41418-020-00658-y](https://doi.org/10.1038/s41418-020-00658-y).

- Abdullah MI, Junit SM, Ng KL, Jayapalan JJ, Karikalan B, Hashim OH. 2019.** Papillary thyroid cancer: genetic alterations and molecular biomarker investigations. *International Journal of Medical Sciences* **16(3)**:450–460 DOI [10.7150/ijms.29935](https://doi.org/10.7150/ijms.29935).
- Antonelli A, Ferrari SM, Fallahi P. 2018.** Current and future immunotherapies for thyroid cancer. *Expert Review of Anticancer Therapy* **18(2)**:149–159 DOI [10.1080/14737140.2018.1417845](https://doi.org/10.1080/14737140.2018.1417845).
- Asano J, Hirakawa A, Hamada C. 2014.** Assessing the prediction accuracy of cure in the Cox proportional hazards cure model: an application to breast cancer data. *Pharmaceutical Statistics* **13(6)**:357–363 DOI [10.1002/pst.1630](https://doi.org/10.1002/pst.1630).
- Ayers M, Lunceford J, Nebozhyn M, Murphy E, Loboda A, Kaufman DR, Albright A, Cheng JD, Kang SP, Shankaran V, Piha-Paul SA, Yearley J, Seiwert TY, Ribas A, McClanahan TK. 2017.** IFN- γ -related mRNA profile predicts clinical response to PD-1 blockade. *Journal of Clinical Investigation* **127(8)**:2930–2940 DOI [10.1172/JCI91190](https://doi.org/10.1172/JCI91190).
- Blangero Y, Rabilloud M, Laurent-Puig P, Le Malicot K, Lepage C, Ecochard R, Taieb J, Subtil F. 2020.** The area between ROC curves, a non-parametric method to evaluate a biomarker for patient treatment selection. *Biometrical Journal* **62(6)**:1476–1493 DOI [10.1002/bimj.201900171](https://doi.org/10.1002/bimj.201900171).
- Burgos JR, Iresjö BM, Smedh U. 2016.** MCG101-induced cancer anorexia-cachexia features altered expression of hypothalamic Nucleob2 and Cartpt and increased plasma levels of cocaine- and amphetamine-regulated transcript peptides. *Oncology Reports* **35(4)**:2425–2430 DOI [10.3892/or.2016.4558](https://doi.org/10.3892/or.2016.4558).
- Cabanillas ME, McFadden DG, Durante C. 2016.** Thyroid cancer. *Lancet* **388(10061)**:2783–2795 DOI [10.1016/S0140-6736\(16\)30172-6](https://doi.org/10.1016/S0140-6736(16)30172-6).
- Charoentong P, Finotello F, Angelova M, Mayer C, Efremova M, Rieder D, Hackl H, Trajanoski Z. 2017.** Pan-cancer immunogenomic analyses reveal genotype-immunophenotype relationships and predictors of response to checkpoint blockade. *Cell Reports* **18(1)**:248–262 DOI [10.1016/j.celrep.2016.12.019](https://doi.org/10.1016/j.celrep.2016.12.019).
- Chen DS, Mellman I. 2017.** Elements of cancer immunity and the cancer-immune set point. *Nature* **541(7637)**:321–330 DOI [10.1038/nature21349](https://doi.org/10.1038/nature21349).
- Chen YP, Wang YQ, Lv JW, Li YQ, Chua MLK, Le QT, Lee N, Colevas AD, Seiwert T, Hayes DN, Riaz N, Vermorken JB, O’Sullivan B, He QM, Yang XJ, Tang LL, Mao YP, Sun Y, Liu N, Ma J. 2019.** Identification and validation of novel microenvironment-based immune molecular subgroups of head and neck squamous cell carcinoma: implications for immunotherapy. *Annals of Oncology* **30(1)**:68–75 DOI [10.1093/annonc/mdy470](https://doi.org/10.1093/annonc/mdy470).
- Coley WB. 1991.** The treatment of malignant tumors by repeated inoculations of erysipelas. With a report of ten original cases. 1893. *Clinical Orthopaedics and Related Research* **262**:3–11.
- Crespo J, Sun H, Welling TH, Tian Z, Zou W. 2013.** T cell energy, exhaustion, senescence, and stemness in the tumor microenvironment. *Current Opinion in Immunology* **25(2)**:214–221 DOI [10.1016/j.coi.2012.12.003](https://doi.org/10.1016/j.coi.2012.12.003).
- David CC, Jacobs DJ. 2014.** Principal component analysis: a method for determining the essential dynamics of proteins. *Methods in Molecular Biology* **1084**:193–226 DOI [10.1007/978-1-62703-658-0_11](https://doi.org/10.1007/978-1-62703-658-0_11).
- Deng S, Wu Q, Yu K, Zhang Y, Yao Y, Li W, Deng Z, Liu G, Li W, Lian Z. 2012.** Changes in the relative inflammatory responses in sheep cells overexpressing of toll-like receptor 4 when stimulated with LPS. *PLOS ONE* **7(10)**:e47118 DOI [10.1371/journal.pone.0047118](https://doi.org/10.1371/journal.pone.0047118).
- Gao HF, Chen LY, Cheng CS, Chen H, Meng ZQ, Chen Z. 2019.** SLC5A1 promotes growth and proliferation of pancreatic carcinoma via glucose-dependent AMPK/mTOR signaling. *Cancer Management and Research* **11**:3171–3185 DOI [10.2147/CMAR.S195424](https://doi.org/10.2147/CMAR.S195424).

- Hänzelmann S, Castelo R, Guinney J. 2013. GSVA: gene set variation analysis for microarray and RNA-seq data. *BMC Bioinformatics* 14:7 DOI 10.1186/1471-2105-14-7.
- Kalathil SG, Thanavala Y. 2021. Importance of myeloid derived suppressor cells in cancer from a biomarker perspective. *Cellular Immunology* 361:104280 DOI 10.1016/j.cellimm.2020.104280.
- Kanazawa S, Kammori M. 2019. Case report: 84-month disease-free survival after surgery for anaplastic thyroid carcinoma. *Journal of Nippon Medical School* 86(1):38–42 DOI 10.1272/jnms.JNMS.2019_86-7.
- Ke ZB, Wu YP, Huang P, Hou J, Chen YH, Dong RN, Lin F, Wei Y, Xue XY, Ng CF, Xu N. 2020. Identification of novel genes in testicular cancer microenvironment based on ESTIMATE algorithm-derived immune scores. *Journal of Cellular Physiology* DOI 10.1002/jcp.29898.
- Khaled YS, Ammori BJ, Elkord E. 2013. Myeloid-derived suppressor cells in cancer: recent progress and prospects. *Immunology and Cell Biology* 91(8):493–502 DOI 10.1038/icb.2013.29.
- Konishi T, Matsukuma S, Fuji H, Nakamura D, Satou N, Okano K. 2019. Principal component analysis applied directly to sequence matrix. *Scientific Reports* 9(1):19297 DOI 10.1038/s41598-019-55253-0.
- Leach DR, Krummel MF, Allison JP. 1996. Enhancement of antitumor immunity by CTLA-4 blockade. *Science* 271(5256):1734–1736 DOI 10.1126/science.271.5256.1734.
- Lechner MG, Megiel C, Russell SM, Bingham B, Arger N, Woo T, Epstein AL. 2011. Functional characterization of human Cd33+ and Cd11b+ myeloid-derived suppressor cell subsets induced from peripheral blood mononuclear cells co-cultured with a diverse set of human tumor cell lines. *Journal of Translational Medicine* 9(1):90 DOI 10.1186/1479-5876-9-90.
- Lee P. 2008. Risk-score system for mathematical calculations in intravenous therapy. *Nursing Standard* 22(33):35–42 DOI 10.7748/ns2008.04.22.33.35.c6465.
- Lei S, Yang J, Chen C, Sun J, Yang L, Tang H, Yang T, Chen A, Zhao H, Li Y, Du X. 2016. FLIP (L) is critical for aerobic glycolysis in hepatocellular carcinoma. *Journal of Experimental & Clinical Cancer Research* 35(1):79 DOI 10.1186/s13046-016-0358-3.
- Lloyd RV, Buehler D, Khanafshar E. 2011. Papillary thyroid carcinoma variants. *Head and Neck Pathology* 5(1):51–56 DOI 10.1007/s12105-010-0236-9.
- Luo D, Chen H, Li X, Lu P, Long M, Peng X, Lin S, Tan L, Zhu Y, Ouyang N, Li H. 2017. Activation of the ROCK1/MMP-9 pathway is associated with the invasion and poor prognosis in papillary thyroid carcinoma. *International Journal of Oncology* 51(4):1209–1218 DOI 10.3892/ijo.2017.4100.
- Mansbach RA, Leus IV, Mehla J, Lopez CA, Walker JK, Rybenkov VV, Hengartner NW, Zgurskaya HI, Gnanakaran S. 2020. Machine learning algorithm identifies an antibiotic vocabulary for permeating gram-negative bacteria. *Journal of Chemical Information and Modeling* 60(6):2838–2847 DOI 10.1021/acs.jcim.0c00352.
- Mojica L, Luna-Vital DA, Gonzalez de Mejia E. 2018. Black bean peptides inhibit glucose uptake in Caco-2 adenocarcinoma cells by blocking the expression and translocation pathway of glucose transporters. *Toxicology Reports* 5(2):552–560 DOI 10.1016/j.toxrep.2018.04.007.
- Ringnér M. 2008. What is principal component analysis? *Nature Biotechnology* 26(3):303–304 DOI 10.1038/nbt0308-303.
- Sato H, Taketomi Y, Ushida A, Isogai Y, Kojima T, Hirabayashi T, Miki Y, Yamamoto K, Nishito Y, Kobayashi T, Ikeda K, Taguchi R, Hara S, Ida S, Miyamoto Y, Watanabe M, Baba H, Miyata K, Oike Y, Gelb MH, Murakami M. 2014. The adipocyte-inducible secreted phospholipases PLA2G5 and PLA2G2E play distinct roles in obesity. *Cell Metabolism* 20(1):119–132 DOI 10.1016/j.cmet.2014.05.002.

- Scouten WT, Francis GL. 2006. Thyroid cancer and the immune system: a model for effective immune surveillance. *Expert Review of Endocrinology & Metabolism* **1**(3):353–366 DOI [10.1586/17446651.1.3.353](https://doi.org/10.1586/17446651.1.3.353).
- Subramanian A, Tamayo P, Mootha VK, Mukherjee S, Ebert BL, Gillette MA, Paulovich A, Pomeroy SL, Golub TR, Lander ES, Mesirov JP. 2005. Gene set enrichment analysis: a knowledge-based approach for interpreting genome-wide expression profiles. *Proceedings of the National Academy of Sciences* **102**(43):15545–15550 DOI [10.1073/pnas.0506580102](https://doi.org/10.1073/pnas.0506580102).
- Tibshirani RJ. 2009. Univariate shrinkage in the cox model for high dimensional data. *Statistical Applications in Genetics and Molecular Biology* **8**(1):1–18 DOI [10.2202/1544-6115.1438](https://doi.org/10.2202/1544-6115.1438).
- Varricchi G, Loffredo S, Marone G, Modestino L, Fallahi P, Ferrari SM, de Paulis A, Antonelli A, Galdiero MR. 2019. The immune landscape of thyroid cancer in the context of immune checkpoint inhibition. *International Journal of Molecular Sciences* **20**(16):3934 DOI [10.3390/ijms20163934](https://doi.org/10.3390/ijms20163934).
- Wang M, Huang S, Chen Z, Han Z, Li K, Chen C, Wu G, Zhao Y. 2020. Development and validation of an RNA binding protein-associated prognostic model for hepatocellular carcinoma. *BMC Cancer* **20**(1):1136 DOI [10.1186/s12885-020-07625-3](https://doi.org/10.1186/s12885-020-07625-3).
- Weber R, Groth C, Lasser S, Arkhypov I, Petrova V, Altevogt P, Utikal J, Umansky V. 2021. IL-6 as a major regulator of MDSC activity and possible target for cancer immunotherapy. *Cellular Immunology* **359**:104254 DOI [10.1016/j.cellimm.2020.104254](https://doi.org/10.1016/j.cellimm.2020.104254).
- Wilkerson MD, Hayes DN. 2010. ConsensusClusterPlus: a class discovery tool with confidence assessments and item tracking. *Bioinformatics* **26**(12):1572–1573 DOI [10.1093/bioinformatics/btq170](https://doi.org/10.1093/bioinformatics/btq170).
- Xie Z, Li X, He Y, Wu S, Wang S, Sun J, He Y, Lun Y, Zhang J. 2020. Immune cell confrontation in the papillary thyroid carcinoma microenvironment. *Frontiers in Endocrinology* **11**:570604 DOI [10.3389/fendo.2020.570604](https://doi.org/10.3389/fendo.2020.570604).
- Xing Q, Liu S, Jiang S, Li T, Wang Z, Wang Y. 2020. Prognostic model of 10 immune-related genes and identification of small molecule drugs in bladder urothelial carcinoma (BLCA). *Translational Andrology and Urology* **9**(5):2054–2070 DOI [10.21037/tau-20-696](https://doi.org/10.21037/tau-20-696).
- Yi M, Nissley DV, McCormick F, Stephens RM. 2020. ssGSEA score-based Ras dependency indexes derived from gene expression data reveal potential Ras addiction mechanisms with possible clinical implications. *Scientific Reports* **10**(1):10258 DOI [10.1038/s41598-020-66986-8](https://doi.org/10.1038/s41598-020-66986-8).
- You X, Yang S, Sui J, Wu W, Liu T, Xu S, Cheng Y, Kong X, Liang G, Yao Y. 2018. Molecular characterization of papillary thyroid carcinoma: a potential three-lncRNA prognostic signature. *Cancer Management and Research* **10**:4297–4310 DOI [10.2147/CMAR.S174874](https://doi.org/10.2147/CMAR.S174874).
- Zarkesh M, Zadeh-Vakili A, Akbarzadeh M, Fanaei SA, Hedayati M, Azizi F. 2018. The role of matrix metalloproteinase-9 as a prognostic biomarker in papillary thyroid cancer. *BMC Cancer* **18**(1):1199 DOI [10.1186/s12885-018-5112-0](https://doi.org/10.1186/s12885-018-5112-0).
- Zeng CM, Chang LL, Ying MD, Cao J, He QJ, Zhu H, Yang B. 2017. Aldo-Keto reductase AKR1C1-AKR1C4: functions, regulation, and intervention for anti-cancer therapy. *Frontiers in Pharmacology* **8**:119 DOI [10.3389/fphar.2017.00119](https://doi.org/10.3389/fphar.2017.00119).
- Zhang W, Sun W, Qin Y, Wu C, He L, Zhang T, Shao L, Zhang H, Zhang P. 2019. Knockdown of KDM1A suppresses tumour migration and invasion by epigenetically regulating the TIMP1/MMP9 pathway in papillary thyroid cancer. *Journal of Cellular and Molecular Medicine* **23**(8):4933–4944 DOI [10.1111/jcmm.14311](https://doi.org/10.1111/jcmm.14311).
- Zhao Z, Li Y, Wu Y, Chen R. 2020. Deep learning-based model for predicting progression in patients with head and neck squamous cell carcinoma. *Cancer Biomarkers* **27**(1):19–28 DOI [10.3233/CBM-190380](https://doi.org/10.3233/CBM-190380).

Zhi J, Yi J, Tian M, Wang H, Kang N, Zheng X, Gao M. 2020. Immune gene signature delineates a subclass of thyroid cancer with unfavorable clinical outcomes. *Aging (Albany NY)* **12(7):**5733–5750 DOI [10.18632/aging.102963](https://doi.org/10.18632/aging.102963).

Zhuang G, Zeng Y, Tang Q, He Q, Luo G. 2020. Identifying M1 macrophage-related genes through a co-expression network to construct a four-gene risk-scoring model for predicting thyroid cancer prognosis. *Frontiers in Genetics* **11:**591079 DOI [10.3389/fgene.2020.591079](https://doi.org/10.3389/fgene.2020.591079).